Applied Catalysis B: Environmental 259 (2019) 118046

Contents lists available at ScienceDirect

Applied Catalysis B: Environmental

journal homepage: www.elsevier.com/locate/apcatb

Simultaneous redox conversion and sequestration of chromate(VI) and arsenite(III) by iron(III)-alginate based photocatalysis

Weifang Zhang[a,b], Feng Liu[a], Yonggang Sun[a,b], Jing Zhang[a,b,*], Zhengping Hao[b]

[a] Key Laboratory of Environmental Nano-Technology and Health Effect, Research Center for Eco-Environmental Sciences, Chinese Academy of Sciences, Beijing 100085, PR China

[b] National Engineering Laboratory for VOCs Pollution Control Materials & Technology, University of Chinese Academy of Sciences, Beijing 101408, PR China

ARTICLE INFO

Keywords:
Fe(III)-alginate hydrogel beads
Chromium
Arsenic
Simultaneous redox conversion
Photocatalysis

ABSTRACT

Multiple heavy-metal ions (e.g. Cr(VI) and As(III)) normally co-exist in acid wastewater, making the wastewater treatment complicated. Herein, the synergistic redox conversion and removal of Cr(VI)/As(III) were effectively achieved by applying iron(III) cross-linking alginate hydrogel beads (Fe-SA) as photocatalyst under simulated sunlight. Results show that not only 100% of the Cr(VI)/As(III) redox conversion was obtained in 150 min at pH 3.0, but also the removal efficiency of the transformed products (Cr(III) and As(V)) was greatly enhanced to above 80% in a wide pH range of 3–7. The $^{\cdot}CO_2^-$ radicals, produced by the ligand to metal charge transfer (LMCT) excitations on Fe-SA, together with the phtocatalysis-generated Fe(II), was responsible for the Cr(VI) reduction. Meanwhile, $^{\cdot}OH$ originating from $^{\cdot}CO_2^-$ mainly contributed to the As(III) oxidation, as confirmed by electron paramagnetic resonance and the by-product of CO_2. Moreover, Fe-SA composite presented excellent reusability and performance in treatment of Cr(VI)/As(III) in real waters.

1. Introduction

The direct discharge of the complex pollutants without appropriate treatment, such as multiple heavy metal ions in acid mining wastewater etc. [1], poses great threats to aquatic life, underground water and human living [2]. Particularly, the co-existing chromium (Cr) and arsenic (As) can be commonly found in acid wastewater from acid mine drainage (AMD), which greatly increases difficulties in the wastewater treatment [3–5].

In general, the mobility, toxicity, bioavailability and environmental fate of Cr and As are largely influenced by their redox speciation. Cr exists in environment as trivalent (Cr(III)) and hexavalent (Cr(VI)) species, in which Cr(VI) is human carcinogen and highly mobile, whereas Cr(III) is non-toxic and can be effectively immobilized by adsorption or precipitation ($Cr(OH)_3$) [6,7]. Arsenic mainly occurs as inorganic forms, namely, in the valence states of As(III) and As(V). As(III) is considered much more toxic and As(V) can be more easily removed through adsorption [8–10]. By applying chemical reagents (e.g. hydrogen peroxide (H_2O_2) [11], Fe^0 [12,13] and Fe(II)/Fe(III) [14,15]) or through the electrocoagulation [16] and photocatalytic methods [17,18], Cr(VI) reduction or As(III) oxidation has been studied individually over the last two decades. However, As(III) and Cr(VI) can co-exist in a variety of environment, including soil, groundwater, biota, and many industrial wastewaters [1,19]. Thus, achieving the simultaneous redox, as well as removal, of Cr(VI) and As(III) in a facile way, should be highly concerned in the environmental remediation.

The direct redox reaction between As(III) and Cr(VI) is negligibly slow when these two ions co-exist in solution [3], although the overall redox reaction is thermodynamically favorable [19], as described Eq. (1).

$$2HCr^{VI}O_4^- + 3HAs^{III}O_2 + 5H^+ \rightarrow 2Cr^{3+} + 3H_2As^{V}O_4^- + 2H_2O,\ \Delta G = -467.95\ kJ/mol \quad (1)$$

In order to accelerate the redox reaction, extra “activating agents” such as H_2O_2 [19], mackinawite (FeS) [20], ferrihydrite [21], and microorganism-bacillus firmus [22] have been used to speed up the redox conversion. As a typical example, H_2O_2 was employed to improve the efficiency of redox transformation, but it can only be realized in acidic conditions, typically at pH 3.0. As pH increases, Cr(VI) is difficult to be reduced by H_2O_2, due to the decrease of the redox potential of CrO_4^{2-}. This will suppress the production of $^{\cdot}OH$ radicals from H_2O_2, and thus slowing down the oxidation of As(III). As a result, an excessive amount of H_2O_2 (e.g. 100 times molar) is needed to increase the redox conversion efficiency of As(III) and Cr(VI) [19]. The redox conversion of As

* Corresponding author at: Key Laboratory of Environmental Nano-Technology and Health Effect, Research Center for Eco-Environmental Sciences, Chinese Academy of Sciences, Beijing 100085, PR China.
E-mail address: jingzhang@rcees.ac.cn (J. Zhang).

https://doi.org/10.1016/j.apcatb.2019.118046
Received 12 April 2019; Received in revised form 26 July 2019; Accepted 1 August 2019
Available online 08 August 2019
0926-3373/

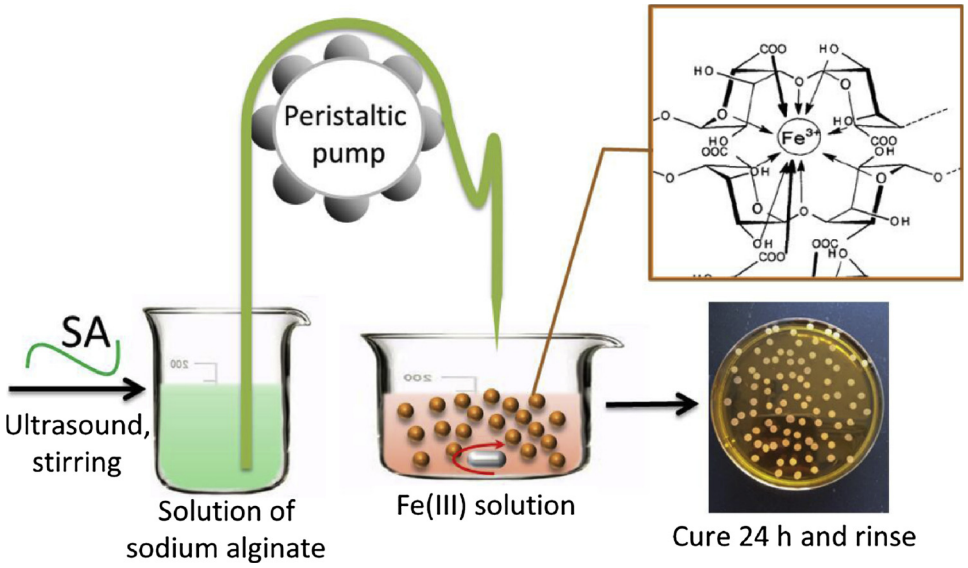

Fig. 1. Schematic diagram of the preparation process of Fe-SA beads.

(III) and Cr(VI) can also occur on the surface of ferrihydrite, but a small amount of these two heavy metal ions can be transformed, due to the limited adsorption capacity of the solid particles [21,23]. Alternatively, external energy was input as the driving force in the conversion, such as electrocatalysis [24], electrical plasma [25], UV irradiation [26], iodide/graphitic carbon nitride based photocatalysis [27,28] and in ice conditions [29]. Although many studies have been exerted to improve the redox conversion efficiency of As(III) and Cr(VI), the simultaneous removal of these two species after transformation is rarely reported. Therefore, the efficient conversion and removal of the multicomponent heavy metals in one-step and a wide range of pH remain a challenge and would be of great significance in environmental remediation.

Photocatalytic technology has been widely investigated and applied in the field of environmental remediation especially water treatment [30], in which photocatalytically produced active species (e.g. photogenerated electron (e^-), hole (h^+)) and oxygen-bearing species ($^{\cdot}OH$, $^{\cdot}HO_2$, and H_2O_2) play a critical role in the redox conversion of toxic pollutants [31]. As an iron-based photocatalyst, Fe(III)-alginate (Fe-SA) complex was made by cross-linking the multivalent Fe(III) with natural, non-hazardous and edible polysaccharide alginate [32]. Previous research demonstrated that Fe-SA has been applied in the degradation of organic dyes [33–37]. In analogy to other Fe(III)-carboxylato complexes, such as Fe-oxalate, Fe-citrate and Fe-malonate [38–40], Fe-SA could initiate the generation of a series of active oxygen species and Fe(II)/Fe(III) ions by the photo-induced ligand to metal charge transfer (LMCT) under light irradiation [41]. These active intermediate species, in principle, can act as redox agents to achieve the decomposition and transformation of multicomponent pollutants by offering both oxidation and reduction effects simultaneously. Hence, it might be feasible to apply Fe-SA photocatalyst in the simultaneous redox conversion of Cr(VI) and As(III) co-existing in wastewater.

Our previous work reported the simultaneous redox and removal of As(III) and Cr(VI) by photocatalysis [42], in which the hybrid photocatalyst of Fe_3O_4/hydrothermal carbon was introduced to accelerate the redox reaction and meanwhile to remove the transformed products by adsorption and precipitation. As Fe_3O_4 is not stable in acid conditions, the redox conversion efficiency and regeneration ability of the hybrid materials are still needed to improve. In this work, photocatalytic transformation of As(III) and Cr(VI) by Fe-SA was studied to realize the simultaneous redox conversion and removal of As(III) and Cr(VI). The Fe-SA catalyst is a hydrogel beads formed by alginate cross-linked with iron ions, and can be stable in solution with a wide range of pH. So, the photocatalyst can consistently provide the photo-generated active intermediates and the solid particle surface for the redox conversion and removal of As(III) and Cr(VI). In this work, the photocatalytic redox kinetics of Cr(VI) and As(III) under simulated sunlight were investigated and the tentative reaction photo-redox mechanism was explored by monitoring the intermediates (Fe(II)/Fe(III)) and active free radicals in the system. $^{\cdot}CO_2^-$ radicals produced by photocatalysis of Fe-SA in our system was first proved to act as the reductive species to effectively convert Cr(VI) into Cr(III), which is especially important for the redox process in neutral and basic conditions. In addition, the bead-like millimeter sized catalyst is favorable to recollection and reusability in applications of environmental remediation.

2. Materials and methods

2.1. Chemicals and materials

All the chemicals were at least of analytical grade, and all solutions were prepared with deionized water. Sodium arsenite ($NaAsO_2$, Merck) and Potassium dichromate ($K_2Cr_2O_7$, 99.8%) were used to prepared As(III) and Cr(VI) stock solution, respectively, and the Cr(VI)/As(III) hybrid solutions were freshly prepared using the stock solutions. Iron(III) nitrate nonahydrate ($Fe(NO_3)_3{\cdot}9H_2O$, ≥99.0%), sodium alginate from brown (SA), tert-Butanol (TBA), 1,0-phenanthroline, HCl, and NaOH were analytical reagents purchased from Sinopharm Chemical Reagent Co., Ltd. in Beijing, China. 5,5-dimethyl-1-pyrroline-*N*-oxide (DMPO, mass percent concentration 97%) was from Aladdin Chemistry Co., Ltd. in China.

2.2. Preparation of Fe-SA hydrogel beads

Iron(III)-alginate hydrogel beads (Fe-SA) were prepared by dropping sodium alginate aqueous solution into iron(III) nitrate solution (Fig. 1) [37]. Briefly, 2 g of sodium alginate powder were dispersed in 100 mL deionized water to obtain the 2% w/v alginate solution. The alginate solution was mixed with a mechanic stirrer until the transparent and viscous solution was obtained. The solution was then added drop-wise using a peristaltic pump (BT100-1L, Longer Pump Co., Ltd., Baoding, China) at a flow rate of 0.5 mL min^{-1} into the 0.3 M $Fe(NO_3)_3$ solution under constant and gentle magnetic stirring. This technique enabled the formation of spherical droplets, which would result in the formation of spherical particles after dispersed in $Fe(NO_3)_3$ solution. The beads were allowed to cure 24 h in $Fe(NO_3)_3$ solution, then rinsed with deionized water and kept in a distilled water bath to remove the

maximum amount of unbound iron, and finally stored in a refrigerator (4 °C).

2.3. Photocatalytic reaction system

The Cr(VI)/As(III) hybrid solution with 96 μM Cr(VI) and 67 μM As (III), 96 μM single Cr(VI) solution and 67 μM single As(III) solution were first prepared as the stock solutions. The pH of the solution was set to a certain value (3.0, 5.0 and 7.0) by adding HCl and then measured with a digital pH meter (FE20, Mettler Toledo Instrumental Co., Ltd, Shanghai, China). Four grams of Fe-SA were mixed with 200 mL of the above stock solutions in a flask under dark condition or under the irradiation of 300 W Xenon lamp (Beijing China Education Au-light Co., Ltd.), which was used to simulate sunlight irradiation. The reaction vessel used for reaction was a 250 mL of glass flask with an opening of 6.5 cm in diameter. The light with the wavelength ranging from 300 to 2500 nm irradiated the solution in the vessel through the opening. The distance (~7 cm) between the Xenon lamp and the solution was maintained and the reaction vessel was cooled with a water-cooling system to keep the reaction temperature at ~25 °C. At the given time intervals, 2 mL of the test solution were sampled from the reaction vessel, filtered through a filter membrane with a 0.22 μm pore size and diluted for analysis. Control experiments without Cr(VI)/As(III) were also conducted under the simulated sunlight to verify the formation of Fe(II) ions in the Fe-SA photo-induced system. All experiments were carried out in solutions that were exposed to the ambient atmosphere (namely, air condition) and hence contained dissolved O_2, unless otherwise noted. In addition, the anoxic and oxic experiments were conducted with O_2 or N_2 (99%) continuously supplied in the whole reaction process. In order to check the effect of free radicals on the conversion of Cr (VI) and As(III), 200 mM of TBA and 5 mM *p*-benzoquinone (*p*-BQ) was used as the scavengers to quench $^{\cdot}OH$ and $^{\cdot}O_2^-$, respectively [28]. Similarly, 5 mM 1,10-phenanthroline were added as Fe(II) quencher to the photo-reaction system with Cr(VI)/As(III) at pH 3.0 [12]. The reuse capability of Fe-SA was also studied by checking the photocatalytic process of fresh Cr(VI)/As(III) solution with the used Fe-SA beads from the previous runs. Note that the used Fe-SA beads were thoroughly washed with distilled water after each run, and the fresh Cr(VI)/As(III) was added before the next run. All experiments were performed in triplicate, and error bars in the figures represent the standard deviation.

To further explore the potential applications of Fe-SA, photocatalytic experiments were carried out using three different water sources, including lake river, irrigation river and ground river, with the addition of 96 μM Cr(VI) and 67 μM As(III)). These waters were collected from different locations in China. The details of water-quality information for the actual water were listed in Table S1.

2.4. Analysis

The concentration of Cr(VI) in the filtrates was analyzed by the 1,5-diphenylcarbohydrazide spectrophotometric method. In the measurement, the filtrate was treated with 1,5-diphenylcarbohydrazide in an acidic medium and Cr(VI) was quantified at 540 nm with a UV–vis spectrophotometer (TU-1810, Persee, China). The total Cr quantity was determined by ICP-OES (Perkin-Elmer Optima 8300, USA) analysis. The initial Cr(VI) concentration was measured to testify the validity of these two methods applied in this study and the data were shown in Table S2. The contents of Fe(II) and total Fe ions were analyzed spectrophotometrically at 510 nm using phenanthroline method. Prior to the sample measurement, 1 mL of methanol was immediately added into the solution to quench the free radicals. The concentrations of As(III) and As(V) were determined by a high performance liquid chromatography-atomic fluorescence (HPLC-AFS) in order to study the oxidation of As(III) into As(V) [43]. In this HPLC-AFS method, PRP-X100 anion exchange column was used for the separation of two As oxidation states, which was subsequently reduced by potassium borohydride, and determined by atomic fluorescence spectrometry. The HPLC spectra were shown in Fig. S1. The retention time for As(III) and As(V) are 2.7 and 7.0 min in our systems, and the concentration of As can be deduced from the intensity of peaks.

X-ray diffraction (XRD) measurement was conducted on an X-ray diffractometer (X' Pert^3 Powder, PANalytical, Netherlands). Diffraction data were recorded with Cu-Kα radiation (40 kV, 40 mA) in the continuous scanning mode. The 2θ scan range was from 5° to 80° in the steps of 0.026 with a collection time of 51 s per step. Scanning electron microscope (SEM) was performed with a SU8020 scanning electron microscope equipped with an energy dispersive X-ray spectroscope. Fourier transform infrared spectroscopy (FT-IR) was monitored on the spectrometer (Perkin-Elmer, USA), and the spectra were collected in the range of 4000–400 cm^{-1} at 4 cm^{-1} resolution. Thermogravimetry (TG) and differential thermogravimetry (DTG) analyses were carried out using a TG209F3 thermal analyzer, and the heating rate was 20 K min^{-1} in static air. The light adsorption properties of the complex were evaluated by measuring their diffuse reflectance UV–vis spectra (DRS), which were recorded on a Varian Cary 500 UV–vis-near-IR spectrometer (Varian Inc., Palo Alto, CA, USA) in the 200–800 nm range with $BaSO_4$ as the reflectance standard. Electron paramagnetic resonance (EPR) analysis was measured using a Bruker electron paramagnetic resonance spectrometer (A300-10/12, Germany). The $^{\cdot}OH$ radicals were captured by using DMPO as the scavenger, with the parameters: centerfield 3480.00 × G, microwave frequency 9.79 GHz, power 5.05 mW. The compositions and oxidation states of Fe-SA before and after reaction were determined by X-ray photoelectron spectroscopy (XPS), which were performed on a Thermo Escalab 250XI with Al Kα source operating at 150 W, beam spot 500 μM. The obtained XPS data were analyzed using XPSPeak41 software by Gaussian-Lorentzian curve-fitting method.

CO_2 was detected on-line on the device shown in Fig. S2, by introducing different ratios of nitrogen to oxygen (N_2:O_2 = 1:0, 0:1 and 4:1 presented anaerobic, pure oxygenic and atmospheric environment, respectively) into the reactor. In this experiment, Fe-SA beads were immersed in the target solutions (the Cr(VI)/As(III) solutions of pH 3.0 or 7.0, or the aqueous hybrid solution of pH 3.0) for 1 h, before it was put into the reactor. The concentration of CO_2 was analyzed by an Agilent 7890B gas chromatograph equipped with hydrogen flame ionization detector (Agilent HP-PLOT U column) and thermal conductivity detector (TCD) (Porapak-Q column and 5A molecular sieve column) [44].

3. Results and discussions

3.1. Characterization of Fe-SA hydrogel beads

As displayed in Fig. 2, the SEM images revealed that the surface of the raw Fe-SA hydrogel bead was regularly and smoothly undulating (Fig. 2a), which was so-called insoluble “egg-box” structure [32,36]. The main elements of the raw Fe-SA samples were oxygen, carbon and iron (Fig. 2b), indicating that iron ions, as the cross-linker of the alginate network, were present on the surface of alginate. The XPS spectra for Fe 2p of Fe-SA at the binding energy of 711.4 and 725.4 eV can be attributed to Fe 2p3/2 and Fe 2p1/2 of Fe(III), respectively (Fig. S3). The X-ray diffraction pattern of Fe-SA (Fig. S4) showed that three typical characteristic peaks (14.3°, 21.3° and 37.1°) of SA almost disappeared, after a high concentration of Fe(III) was added to form the Fe complex. This can be ascribed to the formation of Fe-SA network, as reported in the previous literature [35]. FTIR spectrometry of Fe-SA (Fig. S5) showed the typical absorption peaks from the vibrations of the coordination groups on the particle surface. Specifically, the peaks at 3400 and 2930 cm^{-1} were corresponding to the stretching of −OH and −CH vibration, while two peaks at 1600 and 1417 cm^{-1} were assigned to the asymmetric and symmetric stretching vibrations of the carboxyl group (−COO) of alginate molecule, respectively [35]. The calculated

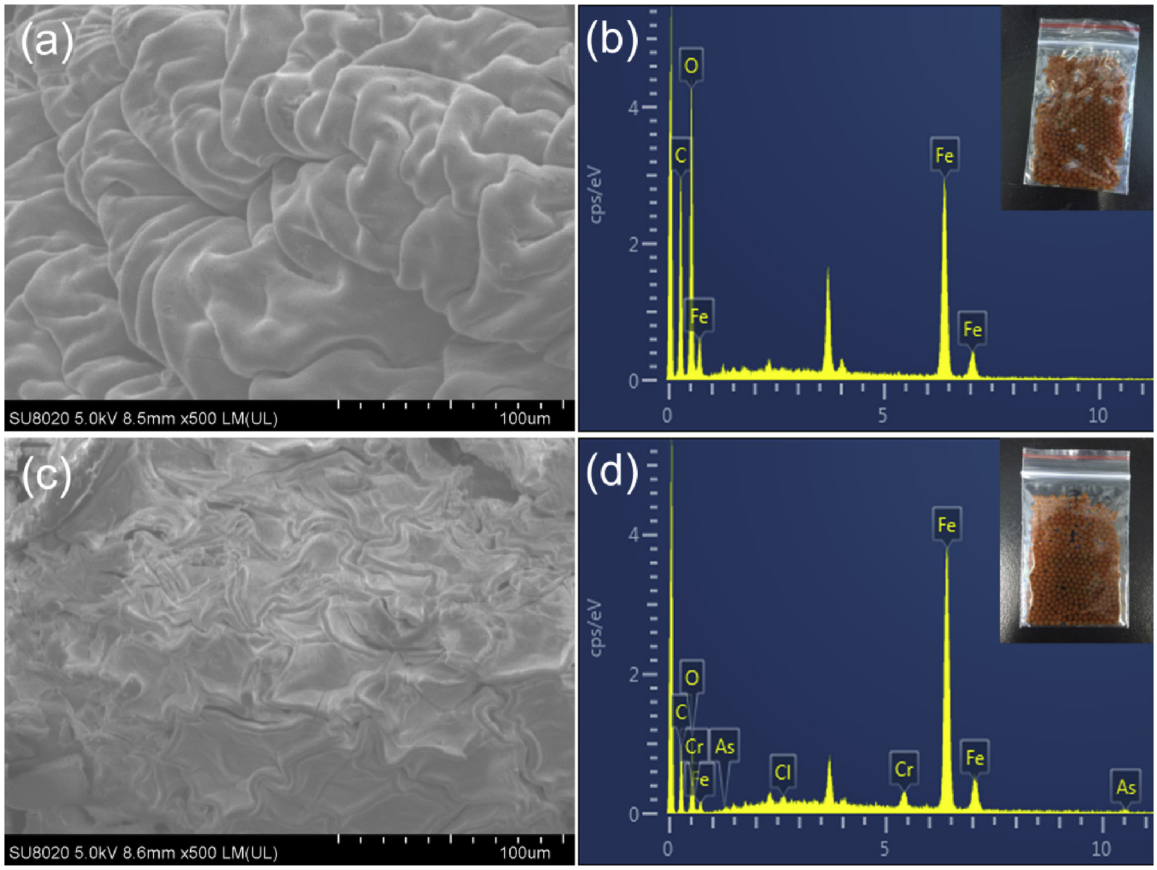

Fig. 2. SEM images (a, c) and elemental spectra (b, d) of the fresh Fe-SA (a, b) and the Fe-SA after treatment of Cr(VI)/As(III) under light irradiation (c, d). Inset: the appearance of the fresh (b) and treated (d) Fe-SA.

moisture content of naturally dry Fe-SA hydrogel beads was 97%. TGA graph of the air-dried Fe-SA displayed that the elemental iron loaded on the dried Fe-SA was 18% in weight, with Fe_2O_3 as the final product (Fig. S6) [45]. UV–vis spectroscopy showed a strong light absorption in the UV and visible light regions for Fe-SA (Fig. S7). This may be ascribed to the *d-d* transitions of the metal ions and the ligand-to-metal charge transfer (LMCT) transitions from alginate toward Fe(III) ion in the complex [35].

3.2. Simultaneous reduction of Cr(VI) and oxidation of As(III)

In the absence of Fe-SA beads, no redox conversion between As(III) and Cr(VI) occurred under light irradiation at pH 3.0 (Fig. S8). In the presence of Fe-SA beads, the photocatalytic reaction of single Cr(VI) or As(III) was first surveyed separately (Fig. S9). In the dark, ~30% Cr(VI) and ~15% As(III) can be removed in their individual system. While under light irradiation, the concentrations of both Cr(VI) and As(III) quickly decreased with time and these two heavy metal ions were completely removed within 60 min at pH 3.0. As pH increased, the removal efficiency of Cr(VI) and As(III) decreased. It suggested that Fe-SA could offer an effective photocatalytic reduction of Cr(VI) and oxidation of As(III), especially in acid conditions.

The removal rate of Cr(VI) was investigated in the Cr(VI)/As(III) coexisting system at different pH values. Fig. 3a revealed that in the dark, about 40% Cr(VI) were removed within 150 min at pH 5.0 and 7.0, while the removal of Cr(VI) increased to 44% at pH 3.0. Under light irradiation, the removal of 96 μM Cr(VI) was complete within 60 min at pH 3.0 in the Cr(VI)/As(III) system. As pH increased, the removal efficiency decreased. Only 41% and 51% Cr(VI) were removed within 60 min at pH 5.0 and pH 7.0, respectively. Fig. 3b displayed the oxidation kinetics of As(III) with the coexisting Cr(VI). In the dark, about 10% As(III) can be removed via adsorption at pH 3.0 and pH 5.0 within 150 min, while the removal efficiency increased to ~30% at pH 7.0 (Fig. 3b). Under light irradiation, the As(III) concentration in Cr(VI)/As(III) solution quickly decreased with time at pH 3.0, and As(III) was completely removed within 90 min. As the pH value increased, As(III) oxidation became slow, and about 80% As(III) can be oxidized at pH 5.0 and pH 7.0 within 150 min. These above results about the simultaneous conversion of Cr(VI) and As(III) revealed that both the Cr(VI) reduction and the As(III) oxidation were markedly accelerated by photocatalysis of Fe-SA, which were more favorable under acidic condition.

Compared to the single Cr(VI) or As(III) system at pH 3.0, the photocatalytic reduction efficiency of Cr(VI) was not influenced by the As(III) existence. However, the oxidation efficiency of As(III) in the presence of Cr(VI) decreased approximately 34% with 60 min. The As(III) oxidation rate constant ($k'_{obs,Air}$) decreased to 0.0166 min^{-1} in the Cr(VI)/As(III) system, smaller than to that of the single As(III) system (0.0374 min^{-1}) (Table S3). The presence of Cr(VI) had an obvious inhibitory effect on the oxidation of As(III) in the Fe-SA photocatalytic system, probably due to the transformation of iron species and/or the suppression of free radicals, which will be discussed later.

In order to check the influence of Cr(VI)/As(III) ratio, the experiments with 144 μM As(III)/96 μM Cr(VI) and 67 μM As(III)/45 μM Cr(VI) were carried out at pH 3.0 under light irradiation. When the concentration of As(III) increased from 67 μM to 144 μM, the removal of 96 μM Cr(VI) was complete within 90 min (Fig. S10a), but the Cr(VI) reduction rate constant ($k_{obs,Air}$) decreased from 0.0557 to 0.0384 min^{-1}. On the other hand, when the concentration of Cr(VI) increased from 45 μM to 96 μM, 67 μM As(III) can still be effectively oxidized within 90 min (Fig. S10b), but the As(III) oxidation rate constant ($k'_{obs,Air}$) decreased from 0.0300 to 0.0166 min^{-1}. The results revealed that the increase of either As(III) or Cr(VI) concentration

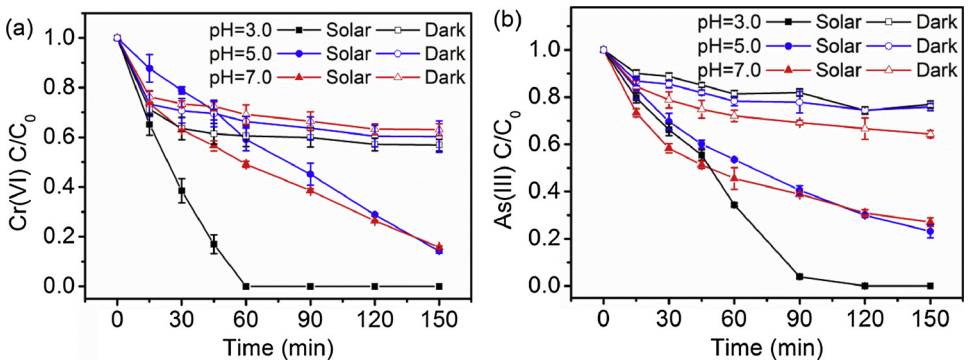

Fig. 3. Concentration change of Cr(VI) (a) and As(III) (b) at various initial pH values in the Cr(VI)/As(III) system with and without light irradiation ([Cr(VI)] = 96 μM and [As(III)] = 67 μM).

resulted in the decrease in the conversion rate of their opponents, probably due to their mutual influence to the intermediate species (free radicals and Fe(II)) in the reaction process.

3.3. Effect of oxygen on the redox conversion of Cr(VI)/As(III)

The effect of oxygen on photo-induced redox of Cr(VI) and As(III) in the Fe-SA system was investigated using a gas purging tube to feed or exclude oxygen with oxygen or nitrogen. The efficiencies of Cr(VI) reduction and As(III) oxidation under the two conditions (oxic or anoxic) were shown in Fig. 4. It can be seen that Cr(VI) photo-reduction could still occur under anoxic/oxic condition. In detail, oxygen had little effect on the Cr(VI) reduction in the Cr(VI)/As(III) system (Fig. 4a), as suggested by the observed reduction rate constant, k_{obs}, from the fit by the pseudo-first-order model ($k_{obs,O2}$ = 0.0529 min^{-1}, $k_{obs,N2}$ = 0.0528 min^{-1}, $k_{obs,Air}$ = 0.0557 min^{-1}, see Fig. S11a and Table S3). However, the As(III) oxidation was significantly accelerated in the presence of oxygen (Fig. 4b). The observed rate constant k'_{obs} of As(III) oxidation under oxic condition ($k'_{obs,O2}$ = 0.0409 min^{-1}) was higher than those under nitrogen and air conditions ($k'_{obs,N2}$ = 0.0131 min^{-1}, $k'_{obs,Air}$ = 0.0166 min^{-1}, see Fig. S11b and Table S3). Specifically, only 54% of As(III) was oxidized within 60 min under nitrogen condition, whereas the oxidation efficiency was promoted to 92% under oxic condition. Similar results about the effect of oxygen on the photocatalytic redox of Cr(VI) and As(III) were also obtained in the single Cr (VI) or As(III) system (Fig. S12). These results suggested that oxygen played an important role in accelerating the photocatalytic oxidation of As(III) by Fe-SA.

3.4. Formation of Fe(II) ions and $^{\cdot}CO_2^-$ radicals and their effects on the Cr (VI) reduction and As(III) oxidation

3.4.1. Reduction mechanism of Cr(VI)

In the Cr(VI)/As(III) system, the concentration of total Fe ions increased with time at pH 3.0 (Fig. 5a), but Fe(II) ions were hardly detected. Similar results were found in the single Cr(VI) system (Fig. S13). As the control experiments, Fe(II) ions from Fe-SA in aqueous solution without any Cr(VI) or As(III) were checked under light irradiation. As shown in Fig. 5b, Fe(II) ions continuously raised with time at pH 3.0, and all the Fe species in solution existed in the form of Fe(II). It indicated that Fe(II) ions could be produced from Fe-SA under light irradiation. This can be explained by the LMCT mechanism, as described in Eq. (2) [41].

$$\text{Fe(III)-SA} + h\nu \rightarrow \text{Fe(II)} + {}^{\cdot}CO_2^{-}\text{-SA} \quad (2)$$

Under light irradiation, the charge transfer from the alginate organo-ligand to Fe(III) resulted in the reduction of Fe(III) to Fe(II), which would be released into the solution at pH 3.0 [46]. When Cr(VI) was present in solution, the dissolved Fe(II) could reduce Cr(VI) into Cr(III) [47], as in Eq. (3).

$$3\text{Fe(II)} + \text{Cr(VI)} \rightarrow 3\text{Fe(III)} + \text{Cr(III)} \quad (3)$$

During this process, Fe(II) ions were consumed and transformed into Fe(III) ions. Therefore, the concentration of Fe(II) was hardly detected in the systems with Cr(VI) and the content of total Fe ions was also low because of the lower solubility of the produced Fe(III) (Fig. 5a).

In order to testify the Fe influences on the redox conversion of Cr (VI) and As(III), Ca-SA was prepared by introducing calcium ions as the favorable cross-linking agents, and the bead was used as Fe-free bare SA for the redox conversion of Cr(VI) and As(III) under light irradiation. It turned out that the redox conversion of Cr(VI) and As(III) was not accelerated by using Ca-SA beads as catalyst (Fig. S14). Further, 5 mM of

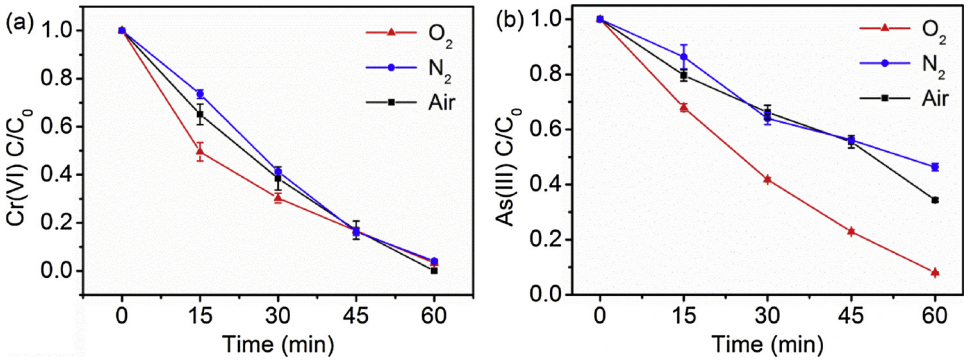

Fig. 4. Concentration change of Cr(VI) (a) and As(III) (b) during photo-induced redox under anoxic (N_2 bubbling), oxic (O_2 bubbling) and air conditions (pH 3.0, [Cr (VI)] = 96 μM and [As(III)] = 67 μM).

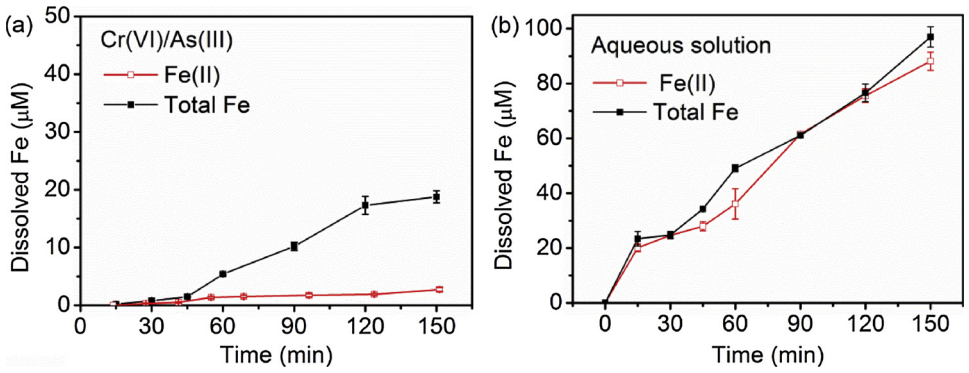

Fig. 5. Concentration change of total Fe and Fe(II) at pH 3.0 under light irradiation in the Fe-SA systems with (a) and without (b) Cr(VI)/As(III).

1,10-phenanthroline were used as Fe(II) quencher in the photo-reaction system with Cr(VI)/As(III) at pH 3.0 [12]. The addition of 1,10-phenanthroline significantly inhibited the Cr(VI) reduction under light irradiation and the Cr(VI) removal efficiency decreased from 100% to 30% within 60 min (Fig. S15). It suggested that the dissolved Fe(II) dominantly contributed to the Cr(VI) reduction at pH 3.0.

According to Eq. (2), carbon-centered radicals ($^{\cdot}CO_2^-$) can also be produced by LMCT of Fe-SA under light irradiation. As verified by the EPR measurement (Fig. 6), the signal of $^{\cdot}CO_2^-$ adduct can be clearly observed in the Fe-SA system both with and without Cr(VI)/As(III) under light irradiation. $^{\cdot}CO_2^-$ is a reductive radical and also an effective electron donor that can reduce different kinds of organic compounds and inorganic metal ions [48]. In the standard state, $E^0(HCr^{VI}O_4^-/Cr^{3+}) = 0.94$ V and $E^0(^{\cdot}CO_2^-/CO_2) = -1.9$ V. So, $\Delta E^0 = (0.94 - (-1.9))$ V = 2.84 V. It indicates that the reaction is spontaneous at acidic condition, and thus $^{\cdot}CO_2^-$ can reduce Cr(VI) to Cr(III), as in Eq. (4). It is worth of note that in the presence of Cr(VI)/As(III), the intensity of $^{\cdot}CO_2^-$ radicals decreased due to the consumption by Cr(VI) (Fig. S16).

$$3\,^{\cdot}CO_2^-\text{-SA} + \text{Cr(VI)} \rightarrow \text{Cr(III)-SA} + 3CO_2 \quad (4)$$

When the initial pH value increased to 5.0 and 7.0, the Fe(II) produced by LMCT was not detected in solution at elevated pH values (Fig. S17), since iron (Fe(II)/Fe(III)) existed in the form of ferric hydroxide on the surface of Fe-SA, rather than released into solution [46]. Although the efficiency of Cr(VI) reduction was relatively lower at pH 5.0 and pH 7.0, compared to that at pH 3.0. Cr(VI) can still be effectively reduced at both pH values (Fig. 3). As verified by the EPR measurement (Fig. S18), the signal of the $^{\cdot}CO_2^-$ adduct can be observed at neutral condition. Moreover, less CO_2 was produced because less Cr(VI) was reduced at pH 7.0 than at pH 3.0, but the amount of CO_2 still increased in the presence of Cr(VI) at pH 7.0 (Fig. S19). It suggested that $^{\cdot}CO_2^-$ radicals were responsible for the reduction of Cr(VI) at pH 5.0 and 7.0. However, the Cr(VI) reduction efficiency was lower at pH 5.0 than pH 7.0. This can be explained by the reason that under neutral condition, the Cr(VI) reduction could occur on the precipitated ferric hydroxide surface by LMCT, through the internal electron from As(III) to Fe(III) on the particle surface [49]. This leads to the increase of the Cr(VI) reduction efficiency at pH 7.0 in Cr(VI)/As(III) system (Fig. 3a). The result is different to the previous work that without light irradiation, Cr (VI) reduction by the surface mediated reaction is enhanced at the lower pH [21,23].

In order to verify the above reaction (Eqs. (2, 4)), the by-product of CO_2 was measured by gas chromatography. As shown in Fig. 7a, CO_2 was clearly detected when exposed to light, while no CO_2 was found when switching off the light. Moreover, a higher content of CO_2 was obtained at low pH (Fig. 7a and Fig. S19a). The results confirmed the role of photocatalysis-produced $^{\cdot}CO_2^-$ radicals in the reduction of Cr (VI). The effect of oxygen on the production of CO_2 was further studied, and it revealed that the content of CO_2 was effectively suppressed by purging N_2 in the system at pH 3.0 (Fig. 7a). This is due to the reason that besides Cr(VI), oxygen can also react with $^{\cdot}CO_2^-$ to produce CO_2, as described in Eq. (5) [50].

$$^{\cdot}CO_2^- + O_2 \rightarrow {}^{\cdot}O_2\text{-} + CO_2 \quad (5)$$

As a comparison, the production of CO_2 was also checked in the absence of Cr(VI)/As(III). As shown in Fig. 7b, there is still a small amount of CO_2 produced in the atmosphere of N_2. The CO_2 would be produced by the redox reaction between light-generated $^{\cdot}CO_2^-$ radicals and Fe-SA complexes, as reported in the Fe(III)-oxalato complexes [51], as in Eq. (6).

$$^{\cdot}CO_2^- + \text{Fe(III)-SA} \rightarrow \text{Fe(II)-SA} + CO_2 \quad (6)$$

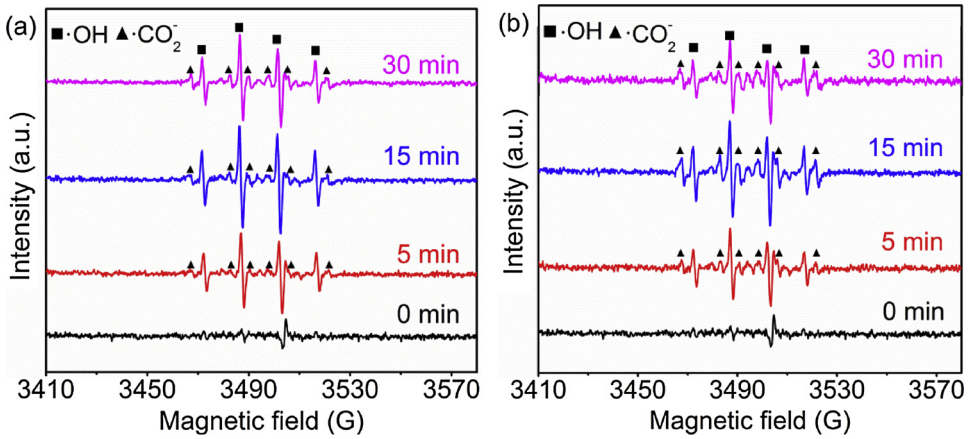

Fig. 6. EPR spectra of DMPO radical adducts formed in the Fe-SA system at pH 3.0 under light irradiation with (a) and without (b) Cr(VI)/As(III).

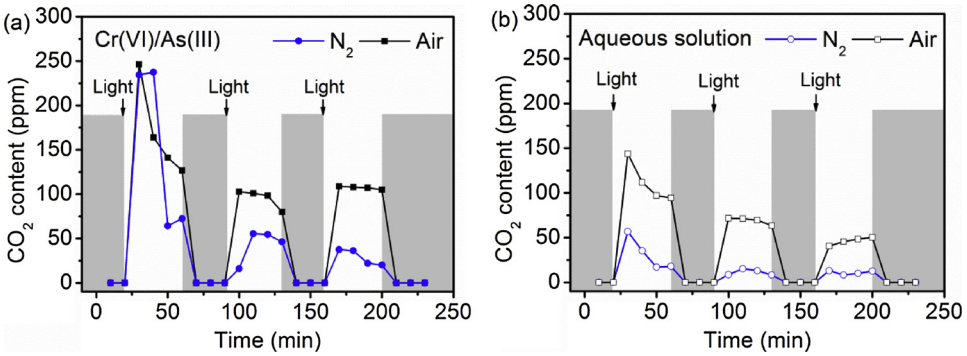

Fig. 7. Production of CO_2 with (white region) or without (grey region) light irradiation at different atmospheres (a) in the Cr(VI)/As(III) system at pH 3.0, and (b) in the aqueous system at pH 3.0.

When in the atmosphere of O_2, the content of the produced CO_2 was much higher than that in the N_2/Air atmosphere (Fig. S19b). Therefore, it again suggested that oxygen can react with $^{\cdot}CO_2^-$ (Eq. (5)). However, more CO_2 was produced in the presence of Cr(VI)/As(III) in the N_2/air atmosphere, compared with the system without Cr(VI) and As (III) (Fig. 7). This further proved the effect of $^{\cdot}CO_2^-$ radicals on the reduction of Cr(VI).

According to Eq. (5), the presence of O_2 could scavenge $^{\cdot}CO_2^-$ radicals, which might affect the reduction of Cr(VI). However, the removal results showed that O_2 has little effect on the reduction of Cr(VI) (Fig. 4a). This can be explained by the reason that the produced $^{\cdot}O_2^-$ (Eq. (5)) can also act as the reductant to transform Cr(VI) into Cr(III) in acid condition [51], as described in Eq. (7).

$$Cr(VI) + 3{}^{\cdot}O_2^- \rightarrow \ldots\rightarrow Cr(III) + 3O_2 \quad (7)$$

where the ellipses represented a multistep transformation from Cr (VI) to Cr(III), e.g. through Cr(V). As a result, the reduction of Cr(VI) was not obviously affected by O_2.

Additionally, the effect of light irradiation on the removal Cr(VI) and As(III) was studied by controlling the switch of light (Fig. S20). It was clearly seen that when the light was switched off, the decreasing rate of the Cr(VI) and As(III) concentrations markedly slowed down. It again suggested that the redox conversion of Cr(VI) and As(III) was accelerated under light irradiation.

3.4.2. Oxidation mechanism of As(III)

On the other hand, the signals of $^{\cdot}OH$ adducts were also distinctively apparent in the EPR spectroscopy in the Fe-SA system under light irradiation (Fig. 6). It has been reported that $^{\cdot}OH$ can be generated from $^{\cdot}CO_2^-$ under acidic conditions, as described in Eqs. (8,9) [41,52]. Both $^{\cdot}CO_2^-$ and Fe(II) can be produced by photocatalysis on Fe-SA, and then, $^{\cdot}O_2^-$ (Eq. (5)) will react with H^+ to generate H_2O_2 in the presence of Fe(II) ions (Eq. (8)). The produced H_2O_2 can react with Fe(II) to form $^{\cdot}OH$ by the Fenton reaction (Eq. (9)) [38]. Subsequently, As(III) was oxidized by $^{\cdot}O_2^-$ or $^{\cdot}OH$, leading to the formation of As(V) (Eqs. (10–12)) [53,54]. Therefore, $^{\cdot}CO_2^-$ was the key radical to initiate the generation of $^{\cdot}O_2^-$ and $^{\cdot}OH$ for the oxidation of As(III).

$$Fe(II) + {}^{\cdot}O_2^- + 2H^+ \rightarrow Fe(III) + H_2O_2 \quad (8)$$

$$Fe(II) + H_2O_2 \rightarrow Fe(III) + OH^- + {}^{\cdot}OH \quad (9)$$

$$As(III) + {}^{\cdot}OH + H^+ \rightarrow As(IV) + H_2O \quad (10)$$

$$As(III) + {}^{\cdot}O_2^- + H^+ \rightarrow As(IV) + HO_2^- \quad (11)$$

$$As(IV) + {}^{\cdot}OH + H^+ \rightarrow As(V) + H_2O \quad (12)$$

In order to study the effect of the free radicals on the As(III) oxidation, TBA and *p*-BQ were used as the scavenger of $^{\cdot}O_2^-$ and $^{\cdot}OH$, respectively. In the single As(III) system (Fig. 8a), the introduction of TBA and *p*-BQ caused the removal efficiency of As(III) markedly decreasing to 31% and 73%, respectively, after 90 min of reaction. It suggested that both $^{\cdot}OH$ and $^{\cdot}O_2^-$ were responsible for the oxidation of As(III), but the former radical contributed more, owing to its higher oxidation ability [19]. In the Cr(VI)/As(III) system (Fig. 8b), TBA and *p*-BQ decreased the removal efficiency of As(III) to 48% and 57%, respectively. Comparing to the single As(III) system, the change of quenching effect in the presence of Cr(VI) was probably due to the reason that the consumption of Fe(II) by Cr(VI), suppressed the production of $^{\cdot}OH$ (Eqs. (8,9)). Therefore, the As(III) oxidation mechanism could be attributed to the reactive oxygen species (ROS) ($^{\cdot}OH$ and $^{\cdot}O_2^-$), where $^{\cdot}OH$ radicals were mainly responsible for As(III) oxidation in the Fe-SA photocatalytic system at pH 3.0.

According to Eq. (5), O_2 is the key factor to accelerate the generation of $^{\cdot}O_2^-$ and $^{\cdot}OH$ for the oxidation of As(III). However, in N_2 condition, the removal of As(III) still occurred in both single As(III) and Cr(VI)/As(III) systems. The XPS characterization of Fe-SA after photo-oxidizing As(III) in N_2 condition (Fig. S21) revealed that the As species adsorbed on the Fe-SA surface were mainly As(V) (binding energy of 45.4 eV), indicating that As(III) (binding energy of 44.4 eV) could still be photo-oxidized without O_2. It has been reported that As(III) can be photo-oxidized on the surface of colloidal ferric hydroxide by ligand to metal charge transfer (LMCT) mechanism [49,55]. Similarly, Fe-SA in our system at pH 3.0 might also provide the solid support and interfaces to trigger LMCT for the oxidation of As(III), since Fe-SA network can act as a photo-responsible complex to initiate photo-catalytic reaction. Therefore, in N_2 condition, As(III) could be photo-oxidized by LMCT through internal electron transfer from As(III) to Fe(III) on the surface of Fe-SA (Eq. (13)). This might also explain that the oxidation of As(III) under light cannot be completely inhibited by free radical quenching experiment.

$$SA\text{-}Fe(III) + As(III) + h\nu \rightarrow 2SA\text{-}Fe(II) + As(V) \quad (13)$$

Not like in the single As(III) system, the oxidation efficiencies of As (III) were similar in air and N_2 condition in the Cr(VI)/As(III) system. This was probably because the presence of Cr(VI) consumed $^{\cdot}CO_2^-$ radicals and decreased the production of active oxygen radicals ($^{\cdot}O_2^-$ and $^{\cdot}OH$). So, in the air condition with a limited oxygen, the oxidation efficiency of As(III) was not obviously increased, as compared to that in N_2 condition, although the rate constant k'_{obs} by fitting for As(III) oxidation under air condition ($k'_{obs,Air} = 0.0166\ min^{-1}$) was slightly higher than that under N_2 conditions ($k'_{obs,N2} = 0.0131\ min^{-1}$).

At pH 5.0 and 7.0, the decrease of dissolved Fe(II) could lead to the loss of $^{\cdot}OH$ (Fig. S18), and thus the oxidation rate of As(III) decreased (Fig. 3b). However, the oxidation of As(III) still proceeded, because ferric hydroxide can adsorb As(III) to form the surface complexation, which can undergo the photo-oxidation of As(III) by LMCT (Eq. (13)). Therefore, As(III) can be effectively oxidized to As(V) at the elevated pH values, even though Fe in the system did not exist in the form of iron ions, as reported in the literature [56].

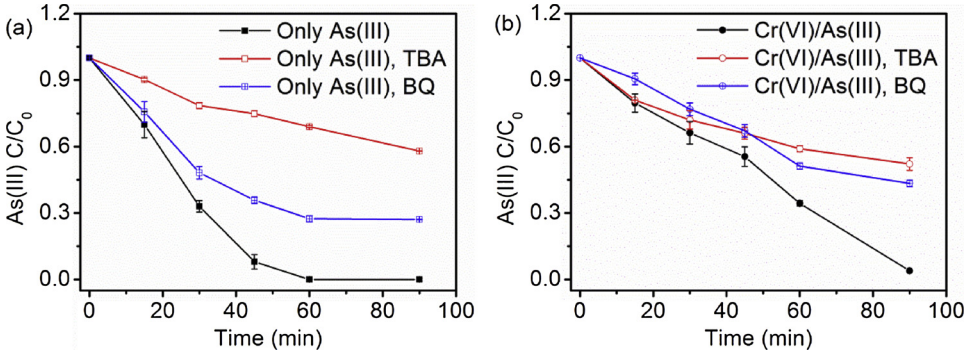

Fig. 8. Quenching effect of TBA and *p*-BQ on the photo-oxidation of As(III) at pH 3.0 in the single As(III) system (a) and the Cr(VI)/As(III) system (b) ([Cr(VI)] = 96 μM, [As(III)] = 67 μM, TBA = 200 mM or *p*-BQ = 5 mM).

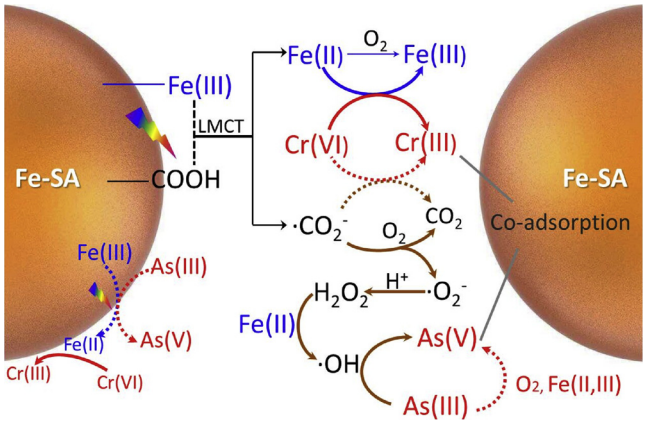

Fig. 9. Schematic illustration of simultaneous conversion of Cr(VI) and As(III) by photocatalysis of Fe-SA.

Based on the above analysis, the mechanism of simultaneous Cr(VI) reduction and As(III) oxidation by Fe-SA through photocatalysis was summarized in Fig. 9, in which the intermediate Fe(II) and $^{\cdot}CO_2^-$ produced from Fe-SA through LMCT were responsible for the reduction of Cr(VI), while $^{\cdot}OH$ originating for $^{\cdot}CO_2^-$ mainly contributed to the oxidation of As(III), especially at a low pH.

3.5. The redox transformation of Cr(VI) and As(III) under dark

In our system, zeta potential demonstrated that the Fe-SA beads were highly negatively charged (Fig. S22), due to the carboxylate groups of SA located on the particle surface [36]. This leads to a weak adsorption of As(III) and Cr(VI) by Fe-SA in single system under dark (Fig. S9). However, the removal efficiency of Cr(VI) or As(III) was both slightly enhanced in the Cr(VI)/As(III) system (Fig. 3). By measuring the species of Cr and As on the particle surface using XPS (Fig. S23), it indicated that under dark conditions, the redox conversion of Cr(VI) into Cr(III) and As(III) into As(V) still occurred on the particle surface at pH 3.0. Especially for Cr(VI), more than 90% of the adsorbed Cr(VI) (binding energy of 579.0 eV) were transformed into Cr(III) (binding energy of 577.0 eV).

The above results suggested that surface adsorption made the redox conversion between Cr(VI) and As(III) energetically favorable, which was coincident with the previous studies [21,23]. A multi-electron transfer process might occur between Cr(VI) and As(III) on the surface of Fe-SA and the ferric hydroxide, where the electrons transferred from the As atoms of Fe–O–As, passed through the solid phase, and eventually reached the Cr atoms of Fe–O–Cr, resulting in the production of As(V) and Cr(III) on the particle surface [21,23]. More ferric hydroxide can precipitate on the Fe-SA surface with the increase of pH, and the precipitated ferric hydroxide was favorable to the adsorption of As. Therefore, a higher adsorption of As(III) on the Fe-SA was obtained at pH 7.0 (Fig. 3b).

3.6. Removal of Cr and As

The concentrations of total Cr and As in the photo-redox system were monitored to check the removal capacity of Fe-SA. As shown in Fig. 10a, the removal of total Cr in the Cr(VI)/As(III) system shared the similar trends as the Cr(VI) reduction (Fig. 3a), where the total Cr was almost removed within 150 min at pH 3.0. However, only ~50% Cr in the single Cr(VI) system were removed within 150 min at pH 3.0 (Fig. S24a), although Cr(VI) had been completely reduced (Fig. S9). This is because that at pH 3.0, Cr^{3+} and $CrOH^{2+}$ ions were the dominant species after reduction, which was hard to precipitate as $Cr(OH)_3$ under acidic conditions (Fig. S25). So, the adsorption of Fe-SA was the main driving force to remove Cr in the Cr(VI)/As(III) system at pH 3.0. In the presence of As, the adsorption of Cr on Fe-SA was increased (Fig. 10a). This might be ascribed to the redox reaction of Cr(VI) and As(III) on the

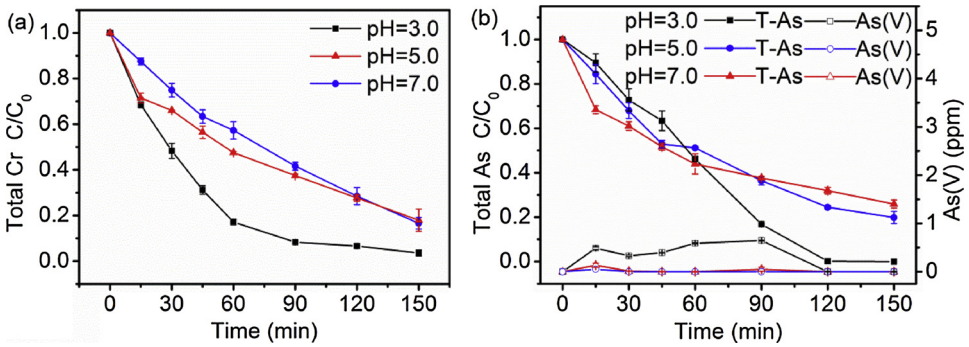

Fig. 10. Concentration change of total Cr (a), total As (T-As) and As (V) (b) in the Cr(VI)/As(III) system under light irradiation ([Cr(VI)] = 96 μM and [As(III)] = 67 μM).

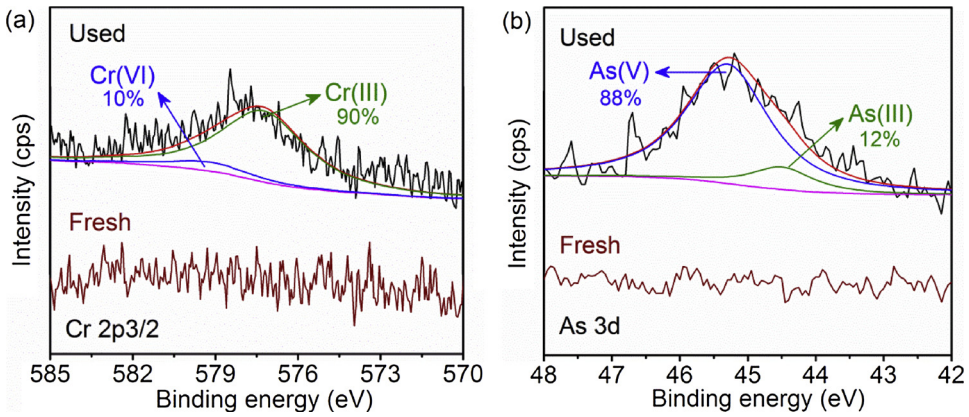

Fig. 11. XPS spectra of Cr (2p3/2) (a) and As (3d) (b) on the Fe-SA before and after the photo-reaction at pH 3.0.

Fe-SA surface, and the absorbed As(V) oxyanion increased the surface negative charge of Fe-SA and thus promoted the adsorption of Cr^{3+}/$CrOH^{2+}$ through electrostatic attraction. After photo-redox treatment, the surface of Fe-SA became rough (Fig. 2c), where Cr and As were detected on the particle surface, as evidenced by energy dispersive spectroscopy (EDS) (Fig. 2d and Fig. S26). The XPS spectra of Fe-SA after the photo-reaction (Fig. 11a) suggested that ~90% Cr(III) and ~10% Cr(VI) were found on the surface of Fe-SA, demonstrating that most of Cr(VI) was reduced to Cr(III).

The removal rate of As was shown in Fig. 10b, by following the change of total As concentration. The total As was completely removed within 120 min at pH 3.0, while the increase of pH caused the decrease in the removal rate of total As. The concentration of As(V) was also measured and shown in Fig. 10b. Only a small amount of As(V) was detected at pH 3.0, while almost no As(V) was found in the solution at the higher pH. Similar results were found in the single As(III) system (Fig. S24b). The results indicated that the produced As(V) was adsorbed by Fe-SA. Combining with the results of As(III) removal by Fe-SA in the dark (Fig. 3b), it can be concluded that As(V) is more likely to be adsorbed on the surface of Fe-SA than As(III), which was consistent with the previous studies [57]. XPS spectra (Fig. 11b) suggested that ~88% As(V) and ~12% As(III) were found on the surface of Fe-SA, demonstrating that As(V) was the main As species sitting on the surface of Fe-SA. In addition, the XPS spectra for Fe 2p after photo-reaction showed that no Fe(II) was found and Fe still presented as the form of Fe(III) on Fe-SA surface (Fig. S3).

3.7. Reuse capacity and implications of Fe-SA

After the photocatalytic reaction, the appearance of Fe-SA, such as shape and color, did not change obviously (inset of Fig. 2d), indicating that the Fe-SA beads are stable for recycling. Therefore, regeneration studies were performed to assess the potential reusability of Fe-SA. As shown in Fig. 12, the conversion efficiency of Cr(VI) was kept 100% even after four cycles, while for As(III), the conversion efficiency slightly decreased to 87%. In addition, the transformed Cr(III) and As (V) can be effectively removed, although the removal efficiency of total Cr and total As continuously decreased with the recycling times (Fig. S27). XPS of Fe-SA after recycling of four times (Fig. S28) suggested that Cr(VI) and As(III) could be effectively transformed into Cr(III) and As(V), respectively. The results revealed that the Fe-SA beads had an excellent cycling stability for the photocatalytic conversion of Cr(VI) and As(III).

Although the surface morphology of Fe-SA beads became rough after use (Fig. 2c), it did not cause an obvious decrease of the redox conversion efficiency after regeneration. This might be because not like inorganic particles, Fe-SA was macromolecular polymer cross-linked by abundant amounts of −COOH and Fe(III). Under light irradiation, the intermediate products such as Fe(II) and free radicals were produced by LMCT between alginate organo-ligand and Fe(III), which was not affected by the surface morphology of the catalyst (Fig. 2c). So, the photocatalytic ability of Fe-SA on the redox of Cr(VI)/As(III) can be kept until the cross-linking structure of Fe-SA is destroyed.

To further verify the feasibility of Fe-SA, real waters (Table S1) spiked with the target metals (Cr(VI) and As(III)) were used to estimate the impact of different matrices on the removal efficiency of Cr(VI)/As (III). Fe-SA showed an excellent capacity of photocatalytic conversion of Cr(VI) and As(III) (Fig. 13 and Fig. S29). Especially at pH 3.0, above 99% Cr(VI) and As(III) were removed under light irradiation in all three waters (irrigation water, ground water and lake water). It suggested that Fe-SA photocatalyst, as the economic and environmentally friendly materials, could be applied in the treatment of acid Cr(VI)/As(III) contained wastewater.

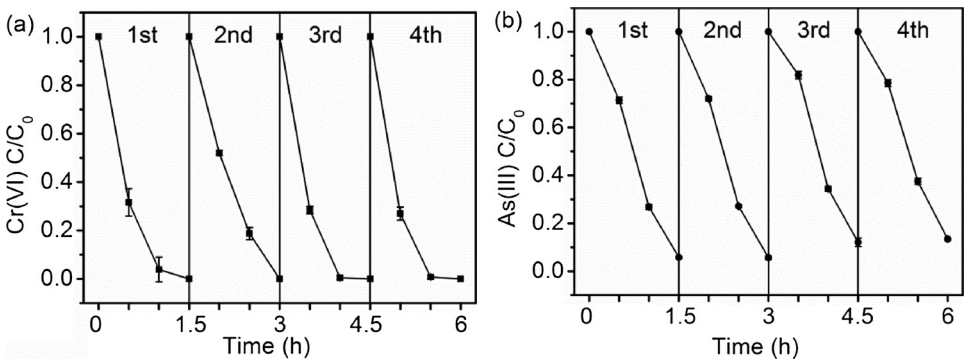

Fig. 12. Recycling of Fe-SA for redox conversion of Cr(VI) (a) and As(III) (b) in the Cr(VI)/As(III) system at pH 3.0.

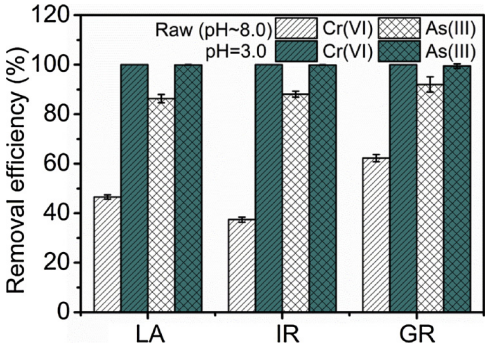

Fig. 13. Removal efficiency of Cr(VI) and As(III) by Fe-SA in real water under light irradiation (LA: lake water, IR: irrigation water, GR: ground water; [Cr (VI)] = 96 μM and [As(III)] = 67 μM).

4. Conclusions

Wastewater normally comprises multiple component contaminants, in which each component might have different physical-chemical behaviors or properties, e.g. different redox characteristics between Cr(VI) and As(III). This brings more difficulties in the wastewater treatment and greatly suppresses the treatment efficiency. In this work, taking co-existing Cr(VI) and As(III) as an example, we developed an effective strategy for the simultaneous reduction of Cr(VI) and oxidation of As (III) via photocatalysis. Fe-SA beads employed as the photocatalyst not only achieve the synergetic redox conversion of Cr(VI) and As(III), but also realize their removal in a wide range of pH. The intermediates of Fe (II) and active free radicals, $^{\cdot}CO_2^-$ and $^{\cdot}OH$, produced by photocatalysis are crucial for the redox conversion of Cr(VI) and As(III). Moreover, the Fe-SA beads exhibit an excellent recycling ability during the processing and high efficiency in the actual wastewater.

Declaration of Competing Interest

The authors declare that they have no known competing financial interests or personal relationships that could have appeared to influence the work reported in this paper.

Acknowledgements

The authors acknowledge the financial support from the National Key Research and Development Program of China (2016YFA0203101 and 2017YFA0207204), the National Natural Science Foundation of China (Grant No. 21876190 and 21836002), the Key Research and Development Program of Ningxia (2017BY064), and the “One Hundred Talents Program” in Chinese Academy of Sciences.

Appendix A. Supplementary data

Supplementary material related to this article can be found, in the online version, at doi:https://doi.org/10.1016/j.apcatb.2019.118046.

References

[1] Z.M. Migaszewski, A. Galuszka, S. Dolegowska, Extreme enrichment of arsenic and rare earth elements in acid mine drainage: case study of Wisniowka mining area (south-central Poland), Environ. Pollut. 244 (2019) 898–906.
[2] J. Ju, J. Kim, L. Vetrakova, J. Seo, D. Heger, C. Lee, H.I. Yoon, K. Kim, J. Kim, Accelerated redox reaction between chromate and phenolic pollutants during freezing, J. Hazard. Mater. 329 (2017) 330–338.
[3] X. Dong, L.Q. Ma, J. Gress, W. Harris, Y. Li, Enhanced Cr(VI) reduction and As(III) oxidation in ice phase: important role of dissolved organic matter from biochar, J. Hazard. Mater. 267 (2014) 62–70.
[4] B. Jiang, Y. Liu, J. Zheng, M. Tan, Z. Wang, M. Wu, Synergetic transformations of multiple pollutants driven by Cr(VI)-sulfite reactions, Environ. Sci. Technol. 49 (2015) 12363–12371.
[5] A. Olenici, S. Blanco, M. Borrego-Ramos, L. Momeu, C. Baciu, Exploring the effects of acid mine drainage on diatom teratology using geometric morphometry, Ecotoxicology 26 (2017) 1018–1030.
[6] H. Fu, Z. Zhou, S. Zheng, Z. Xu, P.J.J. Alvarez, D. Yin, X. Qu, D. Zhu, Dissolved mineral ash generated by vegetation fire is photoactive under the solar spectrum, Environ. Sci. Technol. 52 (2018) 10453–10461.
[7] D.M. Hausladen, A. Alexander-Ozinskas, C. McClain, S. Fendorf, Hexavalent chromium sources and distribution in California groundwater, Environ. Sci. Technol. 52 (2018) 8242–8251.
[8] S. Dixit, J.G. Hering, Comparison of arsenic(V) and arsenic(III) sorption onto iron oxide minerals: implications for arsenic mobility, Environ. Sci. Technol. 37 (2003) 4182–4189.
[9] D. Mohan, C.U. Pittman Jr., Arsenic removal from water/wastewater using adsorbents–a critical review, J. Hazard. Mater. 142 (2007) 1–53.
[10] Y. Mamindy-Pajany, C. Hurel, N. Marmier, M. Romeo, Arsenic (V) adsorption from aqueous solution onto goethite, hematite, magnetite and zero-valent iron: effects of pH, concentration and reversibility, Desalination 281 (2011) 93–99.
[11] K. Kim, J. Kim, A.D. Bokare, W. Choi, H.I. Yoon, J. Kim, Enhanced removal of hexavalent chromium in the presence of H_2O_2 in frozen aqueous solutions, Environ. Sci. Technol. 49 (2015) 10937–10944.
[12] J. Du, J. Bao, C. Lu, D. Werner, Reductive sequestration of chromate by hierarchical FeS@Fe(0) particles, Water Res. 102 (2016) 73–81.
[13] A.B.M. Giasuddin, S.R. Kanel, H. Choi, Adsorption of humic acid onto nanoscale zerovalent iron and its effect on arsenic removal, Environ. Sci. Technol. 41 (2007) 2022–2027.
[14] L. Fernandez-Rojo, M. Hery, P. Le Pape, C. Braungardt, A. Desoeuvre, E. Torres, V. Tardy, E. Resongles, E. Laroche, S. Delpoux, C. Joulian, F. Battaglia-Brunet, J. Boisson, G. Grapin, G. Morin, C. Casiot, Biological attenuation of arsenic and iron in a continuous flow bioreactor treating acid mine drainage (AMD), Water Res. 123 (2017) 594–606.
[15] W. Ding, J. Xu, T. Chen, C. Liu, J. Li, F. Wu, Co-oxidation of As(III) and Fe(II) by oxygen through complexation between As(III) and Fe(II)/Fe(III) species, Water Res. 143 (2018) 599–607.
[16] Y. Hou, H. Liu, X. Zhao, J. Qu, J.P. Chen, Combination of electroreduction with biosorption for enhancement for removal of hexavalent chromium, J. Colloid Interface Sci. 385 (2012) 147–153.
[17] S.H. Yoon, J.H. Lee, S. Oh, J.E. Yang, Photochemical oxidation of As(III) by vacuum-UV lamp irradiation, Water Res. 42 (2008) 3455–3463.
[18] A. Idris, N. Hassan, N.S. Mohd Ismail, E. Misran, N.M. Yusof, A.F. Ngomsik, A. Bee, Photocatalytic magnetic separable beads for chromium (VI) reduction, Water Res. 44 (2010) 1683–1688.
[19] Z. Wang, R.T. Bush, L.A. Sullivan, J. Liu, Simultaneous redox conversion of chromium(VI) and arsenic(III) under acidic conditions, Environ. Sci. Technol. 47 (2013) 6486–6492.
[20] Y.S. Han, C.M. Lee, C.M. Chon, J.A. Kwon, J.H. Park, Y.J. Shin, D.H. Lim, Enhanced oxidation resistance of $NaBH_4$-treated mackinawite (FeS): application to Cr(VI) and As(III) removal, Chem. Eng. J. 353 (2018) 890–899.
[21] E.B. Cerkez, N. Bhandari, R.J. Reeder, D.R. Strongin, Coupled redox transformation of chromate and arsenite on ferrihydrite, Environ. Sci. Technol. 49 (2015) 2858–2866.
[22] S.P. Bachate, V.S. Nandre, N.S. Ghatpande, K.M. Kodam, Simultaneous reduction of Cr(VI) and oxidation of As(III) by Bacillus firmus TE7 isolated from tannery effluent, Chemosphere 90 (2013) 2273–2278.
[23] Z. Ding, F. Fu, D.D. Dionysiou, B. Tang, Coadsorption and subsequent redox conversion behaviors of As(III) and Cr(VI) on Al-containing ferrihydrite, Environ. Pollut. 235 (2018) 660–669.
[24] M. Sun, G. Zhang, Y. Qin, M. Cao, Y. Liu, J. Li, J. Qu, H. Liu, Redox conversion of chromium(VI) and arsenic(III) with the intermediates of chromium(V) and arsenic (IV) via AuPd/CNTs electrocatalysis in acid aqueous solution, Environ. Sci. Technol. 49 (2015) 9289–9297.
[25] B. Jiang, J. Guo, Z. Wang, X. Zheng, J. Zheng, W. Wu, M. Wu, Q. Xue, A green approach towards simultaneous remediations of chromium(VI) and arsenic(III) in aqueous solution, Chem. Eng. J. 262 (2015) 1144–1151.
[26] J. Ryu, D. Monllor-Satoca, D.H. Kim, J. Yeo, W. Choi, Photooxidation of arsenite under 254 nm irradiation with a quantum yield higher than unity, Environ. Sci. Technol. 47 (2013) 9381–9387.
[27] J. Yeo, D. Kim, A.D. Bokare, W. Choi, Photochemical removal of hexavalent chromium through iodide oxidation under 254nm irradiation, Sep. Purif. Technol. 91 (2012) 18–22.
[28] Z. Wang, M. Muruganantham, Y. Zhang, Graphitic carbon nitride based photocatalysis for redox conversion of arsenic(III) and chromium(VI) in acid aqueous solution, Appl. Catal. B: Environ. 248 (2019) 349–356.
[29] K. Kim, W. Choi, Enhanced redox conversion of chromate and arsenite in ice, Environ. Sci. Technol. 45 (2011) 2202–2208.
[30] E. Casbeer, V.K. Sharma, X.-Z. Li, Synthesis and photocatalytic activity of ferrites under visible light: a review, Sep. Purif. Technol. 87 (2012) 1–14.
[31] Y. AlSalka, L.I. Granone, W. Ramadan, A. Hakki, R. Dillert, D.W. Bahnemann, Iron-based photocatalytic and photoelectrocatalytic nano-structures: facts, perspectives, and expectations, Appl. Catal. B: Environ. 244 (2019) 1065–1095.
[32] L. Li, Y. Fang, R. Vreeker, I. Appelqvist, E. Mendes, Reexamining the egg-box model in calcium-alginate gels with X-ray diffraction, Biomacromolecules 8 (2007) 464–468.
[33] Y. Dong, W. Dong, Y. Cao, Z. Han, Z. Ding, Preparation and catalytic activity of Fe alginate gel beads for oxidative degradation of azo dyes under visible light irradiation, Catal. Today 175 (2011) 346–355.
[34] J. Fernandez, M.R. Dhananjeyan, J. Kiwi, Y. Senuma, J. Hilborn, Evidence for Fenton photoassisted processes mediated by encapsulated Fe ions at biocompatible

pH values, J. Phys. Chem. B 104 (2000) 5298–5301.
[35] B. Li, Y. Dong, C. Zou, Y. Xu, Iron(III)–alginate fiber complex as a highly effective and stable heterogeneous Fenton photocatalyst for mineralization of organic dye, Ind. Eng. Chem. Res. 53 (2014) 4199–4206.
[36] R.P. Narayanan, G. Melman, N.J. Letourneau, N.L. Mendelson, A. Melman, Photodegradable iron(III) cross-linked alginate gels, Biomacromolecules 13 (2012) 2465–2471.
[37] H. Titouhi, J.E. Belgaied, Removal of ofloxacin antibiotic using heterogeneous Fenton process over modified alginate beads, J. Environ. Sci. (China) 45 (2016) 84–93.
[38] H. Pang, Q. Zhang, H. Wang, D. Cai, Y. Ma, L. Li, K. Li, X. Lu, H. Chen, X. Yang, J. Chen, Photochemical aging of guaiacol by Fe(III)-oxalate complexes in atmospheric aqueous phase, Environ. Sci. Technol. 53 (2019) 127–136.
[39] Z. Wang, X. Chen, H. Ji, W. Ma, C. Chen, J. Zhao, Photochemical cycling of iron mediated by dicarboxylates: special effect of malonate, Environ. Sci. Technol. 44 (2010) 263–268.
[40] Z. Xu, G. Gao, B. Pan, W. Zhang, L. Lv, A new combined process for efficient removal of Cu(II) organic complexes from wastewater: Fe(III) displacement/UV degradation/alkaline precipitation, Water Res. 87 (2015) 378–384.
[41] J. Chen, W.R. Browne, Photochemistry of iron complexes, Coord. Chem. Rev. 374 (2018) 15–35.
[42] F. Liu, W. Zhang, L. Tao, B. Hao, J. Zhang, Simultaneous photocatalytic redox removal of chromium(VI) and arsenic(III) by hydrothermal carbon-sphere@nano-Fe_3O_4, Environ. Sci. Nano 6 (2019) 937–947.
[43] T. Luo, L. Ye, C. Ding, J. Yan, C. Jing, Reduction of adsorbed As(V) on nano-TiO_2 by sulfate-reducing bacteria, Sci. Total Environ. 598 (2017) 839–846.
[44] H. Yang, C. Ma, X. Zhang, Y. Li, J. Cheng, Z. Hao, Understanding the active sites of Ag/Zeolites and deactivation mechanism of ethylene catalytic oxidation at room temperature, ACS Catal. 8 (2018) 1248–1258.
[45] I.A. Zaafarany, Non-isothermal decomposition of Al, Cr and Fe cross-linked trivalent metal-alginate complexes, J. Nucl. Related Technol. 7 (2010) 84–93.
[46] A. Cruz, L. Couto, S. Esplugas, C. Sans, Study of the contribution of homogeneous catalysis on heterogeneous Fe(III)/alginate mediated photo-Fenton process, Chem. Eng. J. 318 (2017) 272–280.
[47] I.J. Buerge, S.J. Hug, Kinetics and pH dependence of chromium(VI) reduction by iron(II), Environ. Sci. Technol. 31 (1997) 1426–1432.
[48] H. Ren, Z. Hou, X. Han, R. Zhou, Highly reductive radical CO_2^- deriving from a system with SO_4^- and formate anion: Implication for reduction of Cr(VI) from wastewater, Chem. Eng. J. 309 (2017) 638–645.
[49] J. Xu, J. Li, F. Wu, Y. Zhang, Rapid photooxidation of As(III) through surface complexation with nascent colloidal ferric hydroxide, Environ. Sci. Technol. 48 (2014) 272–278.
[50] L.P. Laura, A.B. Marta, A.G. Maria, Yield of carboxyl anion radicals in the photocatalytic degradation of formate over TiO_2 particles, Langmuir 17 (2001) 8422–8427.
[51] S.J. Hug, H.U. Laubscher, B.R. James, Iron(III) catalyzed photochemical reduction of chromium(VI) by oxalate and citrate in aqueous solutions, Environ. Sci. Technol. 31 (1997) 160–170.
[52] N. Chen, H. Shang, S. Tao, X. Wang, G. Zhan, H. Li, Z. Ai, J. Yang, L. Zhang, Visible light driven organic pollutants degradation with hydrothermally carbonized sewage sludge and oxalate via molecular oxygen activation, Environ. Sci. Technol. 52 (2018) 12656–12666.
[53] M. Tong, S. Yuan, S. Ma, M. Jin, D. Liu, D. Cheng, X. Liu, Y. Gan, Y. Wang, Production of abundant hydroxyl radicals from oxygenation of subsurface sediments, Environ. Sci. Technol. 50 (2016) 214–221.
[54] Z. Chen, J. Jin, X. Song, G. Zhang, S. Zhang, Redox conversion of arsenite and nitrate in the UV/Quinone systems, Environ. Sci. Technol. 52 (2018) 10011–10018.
[55] N. Bhandari, R.J. Reeder, D.R. Strongin, Photoinduced oxidation of arsenite to arsenate on ferrihydrite, Environ. Sci. Technol. 45 (2011) 2783–2789.
[56] S.J. Hug, L. Canonica, M. Wegelin, D. Gechter, U. Von Gunten, Solar oxidation and removal of arsenic at circumneutral pH in iron containing waters, Environ. Sci. Technol. 35 (2001) 2114–2121.
[57] A.I. Zouboulis, I.A. Katsoyiannis, Arsenic removal using iron oxide loaded alginate beads, Ind. Eng. Chem. Res. 41 (2002) 6149–6155.